**ORIGINAL PAPER**

Mena Abdelnour · Volkmar Zabel

# Modal identification of structures with a dynamic behaviour characterised by global and local modes at close frequencies

**Abstract** Identification of modal parameters of a space frame structure is a complex assignment due to a large number of degrees of freedom, close natural frequencies, and different vibrating mechanisms. Research has been carried out on the modal identification of rather simple truss structures. So far, less attention has been given to complex three-dimensional truss structures. This work develops a vibration-based methodology for determining modal information of three-dimensional space truss structures. The method uses a relatively complex space truss structure for its verification. Numerical modelling of the system gives modal information about the expected vibration behaviour. The identification process involves closely spaced modes that are characterised by local and global vibration mechanisms. To distinguish between local and global vibrations of the system, modal strain energies are used as an indicator. The experimental validation, which incorporated a modal analysis employing the stochastic subspace identification method, has confirmed that considering relatively high model orders is required to identify specific mode shapes. Especially in the case of the determination of local deformation modes of space truss members, higher model orders have to be taken into account than in the modal identification of most other types of structures.

## 1 Introduction

Space truss structures are a typical solution adopted in previous decades for many civil engineering and aerospace applications, such as bridges, roof structures, and spacecraft systems. The reason for their wide use is not only their lightweight but also their ease of erection and low construction costs. Often, historical space truss structures do not satisfy the current code requirements, and measuring their actual load-bearing capacity would be a proof of the liability of these systems. The stress status of space truss structures is a practical guide to the load-bearing capacity of these systems for further use. Static load testing is a direct and traditional, yet costly, approach to determine the load-bearing capacity of structures. Alternatively, the determination of actual axial forces in the members of a space truss structure can help in the assessment of the remaining load-bearing capacity. Using the dynamic parameters of space frame structures obtained from modal identification, the actual axial forces can be calculated.

In [1,2], the authors used a sensitivity-based method to identify axial forces in space truss structures from dynamic measurements. A methodology for model updating and tension force identification of a two-dimensional truss structure based on modal parameters has been developed by Luong et al. [3]. In the literature, several approaches [4–6] are available to determine axial forces in a beam member based on an estimation

M. Abdelnour (✉) · V. Zabel
Institute of Structural Mechanics, Bauhaus-University, Marienstr. 15, 99423 Weimar, Thuringia, Germany
E-mail: mena.abdelnour@uni-weimar.de

V. Zabel
E-mail: volkmar.zabel@uni-weimar.de

of its bending vibration behaviour. Therefore, the correct identification and assignment of modal parameters for truss structures and their members is mandatory to accurately determine internal forces based on vibration tests. Nevertheless, the identification of the dynamic behaviour of space truss structures has received little attention in the literature so far. Only [7] describes the different vibration mechanisms of space truss structures and provides a comprehensive approach to consider the interference between global and local mechanisms, explained further in Sect. 2.2. Therefore, the motivation behind this research is to accurately identify both the global and local mechanisms of complex space frame structures. Another key aim is to correctly assign experimentally identified modes to numerical modes, by means of automation, during a model updating phase. Achieving these objectives will enable the derivation of the actual axial forces in their members.

In this paper, to determine the modal parameters of a space truss structure, a methodology is developed to identify both local and global vibration behaviours. Numerical modelling provides information on the expected modal parameters, i.e. frequencies and mode shapes. The numerical model is used to identify the type of vibration mechanism based on modal strain energy calculation. Further, an experimental test is performed on a 3-m-long space truss structure to verify the numerical results.

In the following section, we will briefly discuss the theoretical background of methods applied within an identification approach introduced in Sect. 3. The numerical implementation and experimental verification are described in Sects. 4 and 5. The results and findings are then discussed in Sect. 6.

## 2 Theoretical background

Experimental testing is a widely used technique to determine the dynamic behaviour of different types of structures. Many approaches have been developed to perform field testing, for example, experimental modal analysis (EMA). This method depends on measuring both the excitation force and the structural response. An advancement of this method is operational modal analysis (OMA), which only requires the recording of the structural response. The natural or artificial excitation that is unknown [8] should satisfy some assumptions with respect to its statistical properties in time and space.

Especially in terms of larger systems, such as civil structures, OMA is a powerful tool, as practically no technical effort for the generation and recording of an excitation is required [9]. There are many techniques of OMA, which can be categorised into parametric and nonparametric approaches. In addition, one also distinguishes between time-domain and frequency-domain methods. This research adopts the covariance-driven stochastic subspace identification (SSI-cov), a parametric time-domain method based on a stochastic state-space model.

In the next section, a brief overview of the theory behind SSI-cov is given in order to provide background for some of the findings of the present study on a space frame system.

### 2.1 The SSI-cov algorithm

The dynamic behaviour of a multi-degree of freedom system can be described by the well-known system of equations of motion, e.g. [10]:

$$[M]\{\ddot{q}(t)\} + [C_2]\{\dot{q}(t)\} + [K]\{q(t)\} = \{f(t)\} \tag{1}$$

where $\{\ddot{q}(t)\}$, $\{\dot{q}(t)\}$, $\{q(t)\}$, and $\{f(t)\}$ are the acceleration, velocity, displacement, and force vectors, respectively. $[M]$, $[C_2]$, and $[K]$ denote the mass, viscous damping, and stiffness matrices of the system. Equation (1) defines a set of linear second-order differential equations. This set of equations can be transferred into a set of first-order differential equations by a simple extension in the following form [10]:

$$\begin{bmatrix} [C_2] & [M] \\ [M] & [0] \end{bmatrix} \underbrace{\begin{Bmatrix} \{\dot{q}(t)\} \\ \{\ddot{q}(t)\} \end{Bmatrix}}_{\{\dot{s}(t)\}} + \begin{bmatrix} [K] & [0] \\ [0] & [-M] \end{bmatrix} \underbrace{\begin{Bmatrix} \{q(t)\} \\ \{\dot{q}(t)\} \end{Bmatrix}}_{\{s(t)\}} = \begin{bmatrix} [\overline{B}] \\ [0] \end{bmatrix} \{u(t)\} \tag{2}$$

where $\{s(t)\}$ is the state vector and $\{f(t)\}$ is given by $[\overline{B}]$ and $\{u(t)\}$, which defines the location of inputs and the time variation, respectively. One can derive from Eq. (2) in some steps the stochastic discrete-time state-space model, e.g. [9]:

$$\{s_{k+1}\} = [A]\{s_k\} + \{w_k\} \tag{3}$$

$$\{y_k\} = [C]\{s_k\} + \{v_k\} \tag{4}$$

where $\{s_k\}$ is the discrete-time state vector and $k$ denotes the discrete-time instant such that $(t_k = k\Delta t)$. The matrices $[A]$ and $[C]$ are the discrete state matrix and the discrete output matrix, respectively, while $\{y_k\}$ is the sampled observed (i.e. measured) response of the system. The noise vectors $\{w_k\}$ and $\{v_k\}$ represent a combination of the stochastic unknown excitation with process noise in the first case and with measurement noise in the second case.

It can be further shown that the output covariance matrix $[R_i]$ can be composed based on the measured output signals as in Eq. 5, e.g. [10]. Therefore, the matrices [A] and [C], decomposition of $[R_i]$, can be related to the measured output signals as follows:

$$
\begin{aligned}
= E[\{y_{k+i}\}\{y_k\}^T\}] &= [C][A]^{i-1}[G] \\
&= [C][\Psi_c][\Lambda_d]^{i-1}[\Psi_c]^{-1}[G] \\
&= [V][\Lambda_d]^{i-1}[G_m]; \qquad i = 1, 2, \ldots
\end{aligned}
\tag{5}
$$

where $[G]$ is the next state-output covariance matrix that describes the covariance between the system response and the updated state vector. $[\Psi_c]$, $[\Lambda_d]$, $[V]$, and $[G_m]$ are the eigenvector matrix, the eigenvalues diagonal matrix, the modal output matrix, and the modal next state - output covariance matrix, respectively, of the discrete-time state-space model.

As indicated by Equation (5), an appropriate decomposition of the output covariance matrix $[R_i]$ allows for an identification of the matrices $[C]$ and $[A]$. The modal parameters can then be obtained by a subsequent transformation of Equation (5) into modal domain.

In an experimental study, the dimension of matrix [A], i.e. double the number of degrees of freedom (DOF) of the physical system, is unknown. To overcome this problem, it is common practice to compute the solutions assuming a number of different model orders. Therefore, it is also common to represent the results of these model orders in a stabilisation diagram, as shown in Fig. 1. Those poles that occur repetitively as solutions of the respective matrix decomposition are assumed to be related to physical modes. The diagram allows the analyst to select the appropriate parameters related to the physical modes of a given system. In this context, the following stabilisation criteria are applied, as suggested by, e.g. Rainieri and Fabbrocino [9].

$$\frac{|f(\bar{n}) - f(\bar{n} + 1)|}{f(\bar{n})} < 0.01 \tag{6}$$

$$\frac{|\zeta(\bar{n}) - \zeta(\bar{n} + 1)|}{\zeta(n)} < 0.05 \tag{7}$$

$$1 - \text{MAC}(\{\phi(\bar{n})\}, \{\phi(\bar{n} + 1)\}) < 0.02 \tag{8}$$

Here, $f(\bar{n})$, $\zeta(\bar{n})$, and $\{\phi(\bar{n})\}$ are the frequency, damping ratio, and mode shape vector at model order $\bar{n}$. MAC is the model assurance criterion, as given in [11]. Nevertheless, the selection of appropriate poles from a stabilisation diagram is also influenced by further factors that have their origins both in the physical test and data analysis.

For example, some modes are usually more excited than others in a modal test. As given in [9] and [12], the weakly excited modes may appear only at a higher model order. Further, as mentioned earlier, the number of DOF of the considered system, which determines the order of a respective state-space model, is also related to the number of modes that can be excited and identified. Accordingly, identifying modes that require the inclusion of a certain number of DOF in a theoretical model of a structure requires considering a state-space model obtained from experimental data at a respective high order.

## 2.2 Numerical distinction between local and global vibrations

On the one hand, the vibration behaviour of space truss structures is characterised by global deformations of the complete system, for example, plate or beam bending or torsion in the case of truss beams. On the other hand, individual members can deform in local bending patterns.

In order to be able to represent the bending vibrations of individual members numerically, they should be modelled by finite beam elements with a discretisation between the structural nodes. Without intermediate DOF, a deformation of the truss members, i.e. between the structural nodes, cannot be represented. However,
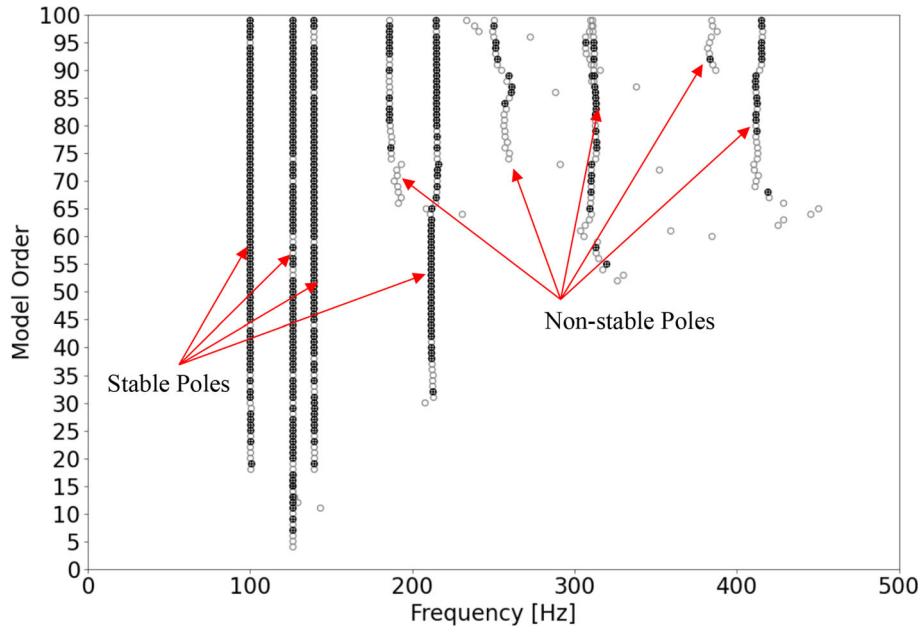
**Fig. 1** Stabilisation diagram related to identification of global frequencies of a space frame structure, presented in this study, of a frequency until 500 Hz, with a model order of 50. (∘) satisfies the pre-defined stability criteria, and (∘) is below these criteria

discretising the truss members into several beam elements can make a clear distinction between global and local mode shapes very difficult.

To distinguish between local and global mode shapes of a numerical model, an approach based on modal strain energy (MSE) was suggested in [7]. The total modal strain energy of a space frame structure is given as, e.g. [13],

$$\text{MSE} = \frac{1}{2}[\Phi]^{\text{T}}[K][\Phi] \tag{9}$$

where $[\Phi]$ and $[K]$ are the modal matrix and the stiffness matrix of the structure, respectively. This relation can also be applied to single elements, i.e. using the element stiffness matrices. Accordingly, the breakdown of the modal strain energy to a single beam element allows for a distinction between axial, bending, torsional, and shear strain energy components.

As the global deformation of truss structures is mainly related to longitudinal forces and strains in the structural members, the contributions of axial strains dominate the total strain energy for these deformation states. On the other hand, local deformation of the members results in bending strain energy. Therefore, calculating the percentage of participation of the axial and bending strain energies to the total strain energy gives a clear understanding of the type of deformation of each vibration mode.

Additionally, the calculation of the modal strain energy shows which DOF are active in each mode shape. This facilitates the selection of relevant DOF, i.e. location and direction of sensors, to be considered in experimental set-ups.

### 2.3 Mode shape pairing

An automated identification of internal member forces requires a correct assignment of numerical modes to respective identified modes, i.e. a method for the distinction between local and global modal components. For this purpose, the energy-based modal assurance criterion (EMAC), proposed in [14], is adopted to ensure correct mode shape pairing in the identification process. The EMAC uses the regular MAC, given in the following equation:

$$\text{MAC}_{xn} = \frac{(\{\Phi\}_x^T\{\Phi\}_n)^2}{(\{\Phi\}_x^T\{\Phi\}_x)(\{\Phi\}_n^T\{\Phi\}_n)} \tag{10}$$

where $\{\Phi\}_n$ and $\{\Phi\}_x$ are the numerical and experimental mode shapes, respectively. Then, the DOF, in the case of any given structure, are separated into $z$ clusters, such that the eigenvector of a mode shape $n$ is written as follows:

$$\{\Phi\}_n^T = [\{\Phi\}_{n1}^T \{\Phi\}_{n2}^T \dots \{\Phi\}_{nz}^T]^T \tag{11}$$

and the corresponding clustered stiffness matrices $K_{rl}$ are given by

$$K = \begin{bmatrix} K_{11} & K_{12} & \dots & K_{1z} \\ K_{21} & K_{12} & \dots & K_{1z} \\ \vdots & \vdots & \ddots & \vdots \\ K_{z1} & K_{z2} & \dots & K_{zz} \end{bmatrix} \tag{12}$$

where $[K]$ is the global stiffness matrix and $\forall r, l = 1, 2 \dots z$. Afterwards, a weighting factor $\Pi_{nr}$, which defines the relative modal strain energy ($\text{MSE}_{nr}$) for each mode $n$ based on a respective cluster $r$ of DOF, is calculated by

$$\Pi_{nr} = \frac{\text{MSE}_{nr}}{\text{MSE}_n} = \frac{\sum_{l=1}^z \{\Phi\}_{nr}^T [K]_{rl} \{\Phi\}_{nl}}{\{\Phi\}_n^T [K] \{\Phi\}_n} \tag{13}$$

where $\text{MSE}_n$ is the total modal strain energy of the same mode $n$ obtained from the numerical model. The EMAC is then calculated, as given in [14] by

$$\text{EMAC}_{xnr} = \Pi_{nr} \times \text{MAC}_{xn} \tag{14}$$

and, similar to the MAC limits, it takes values between zero for no correlation and one showing a high correlation.

## 3 Identification methodology

To correctly determine the modal solution of a space frame structure, the following procedure, shown in Fig. 2, is proposed. The proposed steps target the numerical and experimental identification of local and global modes of space frame structures. The procedure starts by creating a numerical model for a respective space frame structure, using finite beam elements to represent the dynamic behaviour of the members in addition to global structural deformations. By means of the solution of the generalised eigenvalue problem related to the undamped system, the modal parameters are obtained. Based on the modal strain energy calculation, global and local vibration modes are distinguished. Afterwards, using the numerical parameters, a group of DOF is chosen for the experimental modal analyses.

In this study, modal parameters were identified by OMA. Therefore, only the structural response, with no excitation, was measured during the tests, such that measurement data were acquired at the locations of accelerometers, i.e. selected DOF, to capture both local and global modes of the structure. To obtain all desired natural frequencies and mode shapes, a parameter study of the influence of the SSI-cov parameters on the number of identified modal parameters is necessary, for example, the maximal computed model order. Then, using the respective SSI-cov parameters, system and modal identification follows. Finally, using the EMAC criterion, an automatic pairing between numerical and experimental mode shapes is conducted, followed by the MAC values calculation. Identified mode shapes are complex, while the numerical modal analysis of an undamped system results in real-valued modes. To overcome this problem, the real part of the experimental modes was used for the MAC values calculation after a coordinate transformation to minimise the values of the imaginary part. Eventually, selected mode shapes and natural frequencies are provided for subsequent use to determine internal member forces. The proposed methodology has been applied and tested on the space truss structure, shown in Fig. 3. Section 4.1 prescribes the characteristics of the space truss structure of this work.
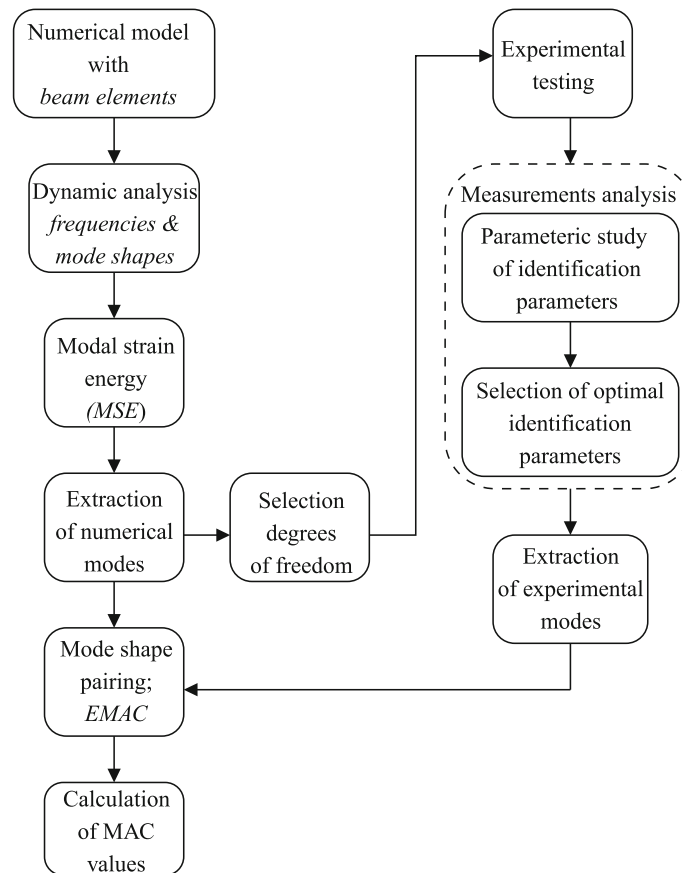
**Fig. 2** Proposed methodology to identify local and global vibrations of space frame structures
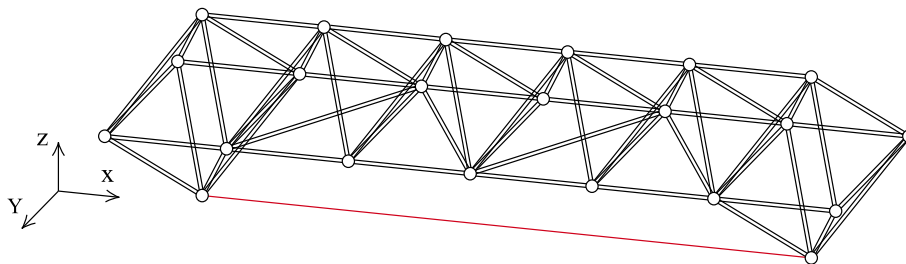


**Fig. 3** Physical truss model with (——) tubular cross section of 22 mm diameter and thickness of 1 mm, (——) threaded rod of 8.9 mm diameter, and MERO standard nodes

## 4 Implementation

### 4.1 Physical model description

The space truss model, shown in Fig. 3, is 3 m long and 0.5 m wide. The main part has a height of 0.353 m. All elements are of a standardised tubular cross section with an external diameter of 22 mm and a 1 mm wall thickness. Apart from the threaded rod that is marked in red in Fig. 2, the structural elements have a length of 0.5 or 0.7 m, depending on their position. The circular cross section of the 2.5-m-long threaded rod has a core diameter of 8.9 mm. Each of the tubular members has a hexagonal connector with an M12 bolt at the two ends. The M12 bolts connect the members with MERO standard nodes. Figure 4 shows the connection detail between the member and the node.
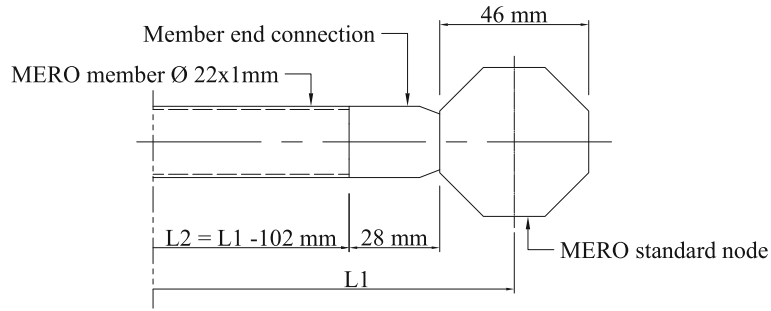
**Fig. 4** Characteristics of MERO member and end connection to MERO standard node

**Table 1** Dimensions of the physical model elements

| Item | Weight (kg) |
| --- | --- |
| 500 mm member | 0.380[1] |
| 707 mm member | 0.480[1] |
| Standard MERO node | 0.235 |

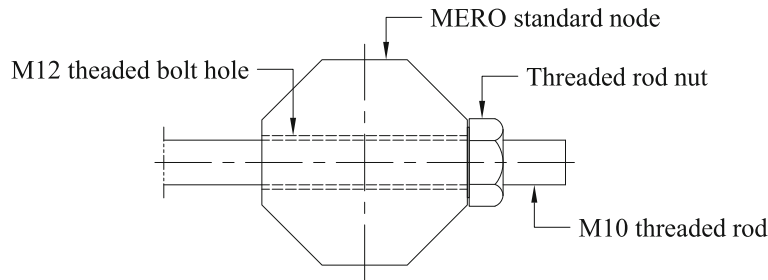[1]The weight of the member includes the end connections weight



**Fig. 5** End connection between the threaded rod and MERO standard node

Due to the end connections of the member, the total weight of a member is higher than a pure tubular cross section. In the numerical model, the length of any member is assumed to cover the distance between the centre lines of the connecting nodes. Table 1 gives the weight of the members and the connecting nodes used in the physical model. The threaded rod has been introduced to provide a possibility to pre-stress the system such that different levels of normal force in the truss members can be achieved by tightening a nut at the rod's end. Figure 5 illustrates how the threaded rod is attached to the MERO node.

Additionally, a non-negligible effect of the mass at the connection nodes on the dynamic behaviour of the system has to be expected. Therefore, the masses of the respective connectors at the rods' ends and of the spherical nodes were taken into account as concentrated masses located at the connection nodes.

## 4.2 Numerical modelling

For the preparation of the experimental tests, a numerical model of the space truss structure, shown in Fig. 3, has been created using the finite element software SOFiSTiK [15]. The modelling of the members of the space truss included finite beam elements using the Timoshenko beam theory. Young's modulus, Poisson's ratio, and density are $2.1 \times 10^5$ N/mm$^2$, 0.3, and 7800 kg/m$^3$, respectively. These parameters are assumed to be known and constant. Each member of the truss was discretised into six beam elements, such that five nodes are always between the structural connecting nodes in the numerical model. The threaded rod was discretised into forty beam elements to reach mesh convergence. To simplify the numerical model, the members are rigidly connected. Possible rotational flexibility in the nodes has not been taken into account as the stiffness of the bolted connection is considered very high regarding the minimal deflections in a modal test.
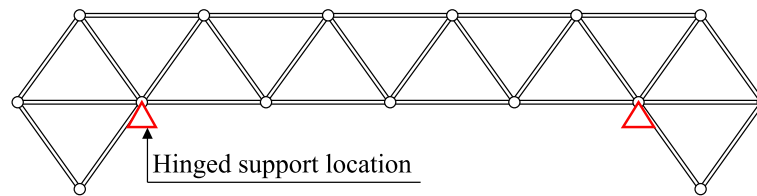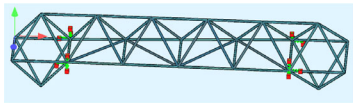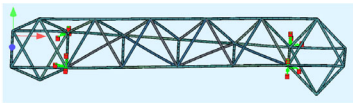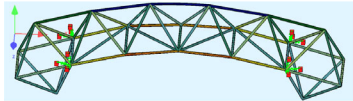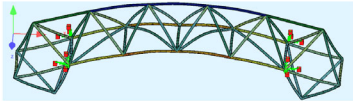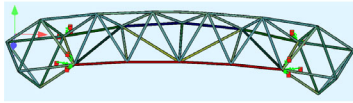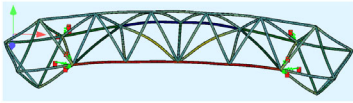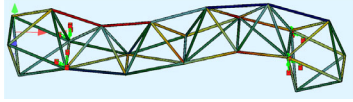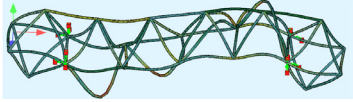
**Fig. 6** Location of hinged supports of the space truss structure (the threaded rod is omitted)

**Table 2** Comparison of the calculated natural frequencies due to free–free support conditions using different discretisations

| Mode | Coarse discretisation | Fine discretisation | Diff. [%] |
|------|------------------------|----------------------|-----------|
| 1 | 97.76 Hz | 97.50 Hz | 0.27 |
| |  |  | |
| 2 | 104.37 Hz | 103.65 Hz | 0.69 |
| |  |  | |
| 3 | 127.43 Hz | 126.28 Hz | 0.91 |
| |  |  | |
| 4 | 213.79 Hz | 195.91 Hz | 8.36 |
| |  |  | |
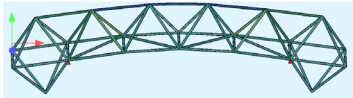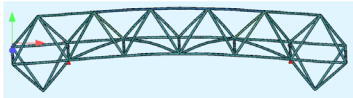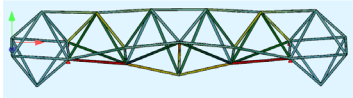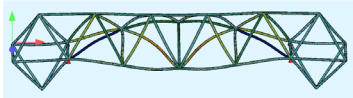
A free–free support condition is assumed and simulated in experimental set-ups by suspending the structure using rubber cords. Such that the experimental boundary conditions, which were chosen to avoid uncontrollable effects from uncertain boundary conditions, could be represented appropriately. In [7], the authors observed for a similar structure as considered here that the computed natural frequencies of the first global mode differed by about 75% between two models with and without discretised truss members in the case of free–free boundary conditions. This p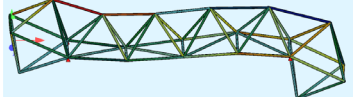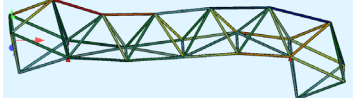henomenon was not observed in the case of a clamped support on the one end of the structure, which gives reason to investigate if similar effects occur with the space truss structure of this study as well.

### 4.2.1 Effect of the free–free boundary condition on the vibration mechanisms

The first four global modes of the case study truss of this work are examined under free–free and hinged–hinged boundary conditions. In the first model, each truss member was modelled by a single beam element (coarse discretisation). Then, in the second model, the members were discretised with five intermediate nodes (fine discretisation). The comparison was carried out without including the threaded rod in the analysis, only the space truss structure. After investigating these two cases for free–free boundary condition, hinged supports were introduced into both models at the locations shown in Fig. 6.

Divergent from the results in [7], the respective natural frequencies obtained for the models with the two considered boundary conditions, as given in Tables 2 and 3, do not deviate in different orders in case of choosing a finer discretisation for the truss members. In fact, the respective relative deviations are even smaller if the system had free–free boundary conditions in most cases. Accordingly, the statement in [7] could not be proven; therefore, such a negative effect of free–free boundary conditions on the numerical results is not expected.

**Table 3** Comparison of the calculated natural frequencies due to hinged–hinged support conditions using different discretisations

| Mode | Coarse discretisation | Fine discretisation | Diff. [%] |
|------|-----------------------|---------------------|-----------|
| 1 | 117.85 Hz | 116.37 Hz | 1.25 |
| |  |  | |
| 2 | 167.42 Hz | 164.18 Hz | 1.94 |
| |  |  | |
| 3 | 172.28 Hz | 169.70 Hz | 1.50 |
| |  |  | |
| 4 | 211.77 Hz | 200.40 Hz | 5.37 |
| |  |  | |

### 4.3 Results of the numerical analysis

The numerical model of the space truss structure is vital to understand the structure's different vibration mechanisms. Due to the free–free boundary conditions, the first six mode shapes are rigid body movements (three translations and three rotations) with frequencies equal to zero Hz. By excluding these modes, the first eighteen mode shapes, extracted from the numerical model with their natural frequencies, are shown in Fig. 7. The numerical outcome shows two vibration mode types, global and local vibrations, which agree with the results given in [7]. If a mode of the complete structure is deformed like a continuum system, the mode shape is considered a global vibration mode. That is to say that the whole structure deformation is higher than any local member deformation. For example, the 11th, 14th, and 15th mode shapes in Fig. 7 are classified as global modes: torsion, lateral bending, and vertical bending.

On the contrary, a mode is classified as local if the deformations of one or several members dominate the system's mode shape. For instance, modes 1 to 10 show local vibrations of the threaded rod (lateral and vertical bending), while the rest of the space truss structure shows barely any deformation. Similarly, modes 12, 16, and 17 illustrate local member bending of the end inverted pyramids along with the threaded rod.

In some cases, it is infeasible to clearly distinguish which type of vibration dominates because the mode is a combination of local member deformations and global vibration. For example, modes 7 and 13 combine global torsion with local member bending of the threaded rod, while mode 18 looks like a second-order global beam bending mode with local member bending.

Concerning this issue, the global vibration of a space truss structure is related to the axial deformations of the members. On the other hand, local member vibration corresponds to a bending deformation of the member. Thus, as implied in [7], a separation between the two types of vibration is possible based on the modal strain energies, namely axial and bending strain energies of the truss members.

Accordingly, the percentage of participation of either axial or bending strain energies to the total modal strain energy of a space truss structure can be used as an indicator to distinguish between global and local modes. As given in Table 4, $U_a/U_t$ and $U_b/U_t$ are the axial modal strain energy and bending strain energy ratios, respectively, where $U_a$, $U_b$, and $U_t$ are the axial, bending, and total modal strain energies, respectively.

For example, in the case of the 7th and 13th modes, the bending modal strain energy is much higher than the axial. Thus, these modes can be considered as dominated by local member vibrations. The case is reversed in mode 15, where the axial modal strain energy surpasses the bending, implying that this mode is a global vibration. In the case of mode 18, the contributions of axial strain and local bending to the total
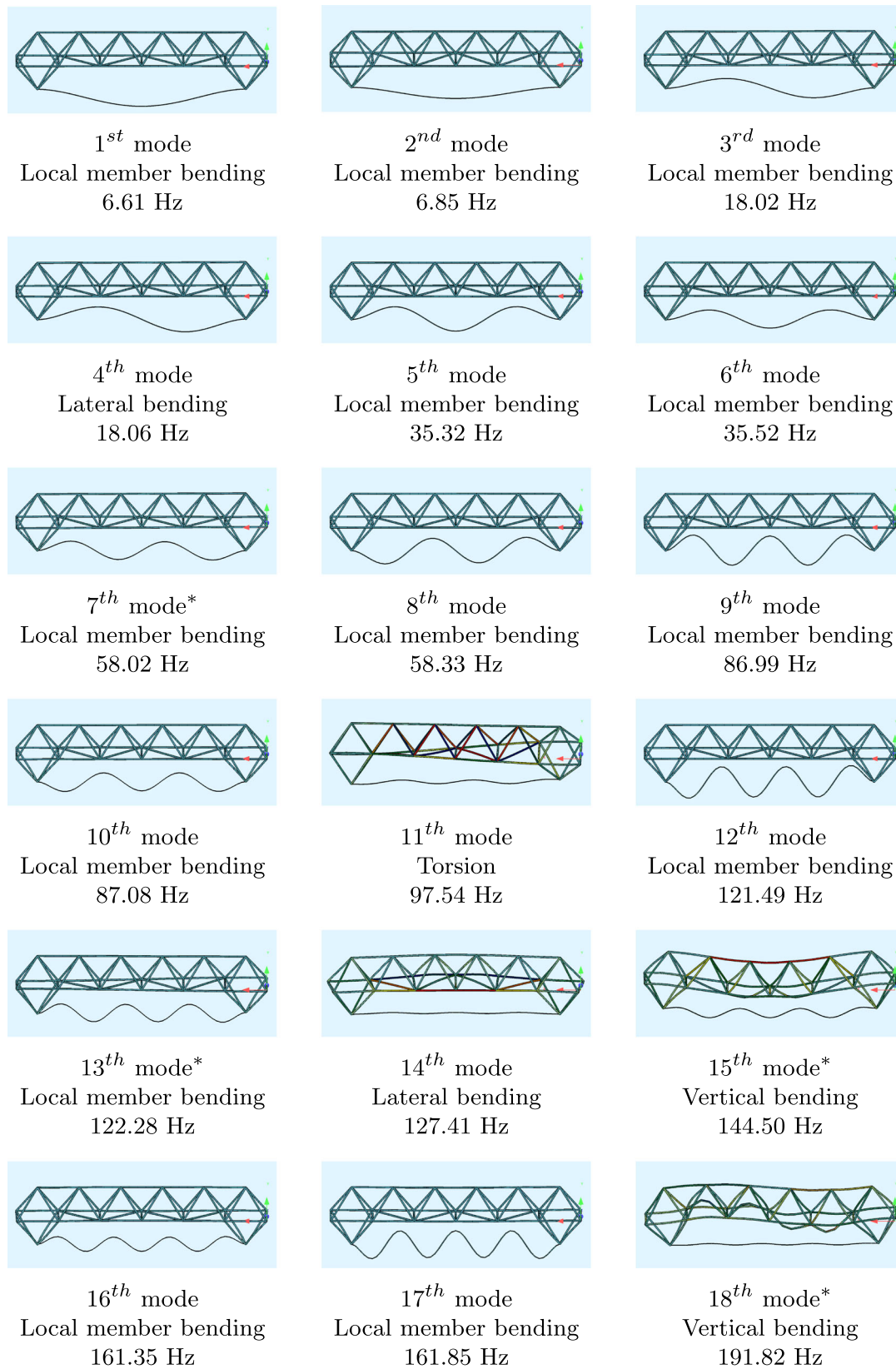
$1^{st}$ mode
Local member bending
6.61 Hz

$2^{nd}$ mode
Local member bending
6.85 Hz

$3^{rd}$ mode
Local member bending
18.02 Hz

$4^{th}$ mode
Lateral bending
18.06 Hz

$5^{th}$ mode
Local member bending
35.32 Hz

$6^{th}$ mode
Local member bending
35.52 Hz

$7^{th}$ mode*
Local member bending
58.02 Hz

$8^{th}$ mode
Local member bending
58.33 Hz

$9^{th}$ mode
Local member bending
86.99 Hz

$10^{th}$ mode
Local member bending
87.08 Hz

$11^{th}$ mode
Torsion
97.54 Hz

$12^{th}$ mode
Local member bending
121.49 Hz

$13^{th}$ mode*
Local member bending
122.28 Hz

$14^{th}$ mode
Lateral bending
127.41 Hz

$15^{th}$ mode*
Vertical bending
144.50 Hz

$16^{th}$ mode
Local member bending
161.35 Hz

$17^{th}$ mode
Local member bending
161.85 Hz

$18^{th}$ mode*
Vertical bending
191.82 Hz

**Fig. 7** First eighteen numerical mode shapes of the space truss structure with their natural frequencies. (*) These modes include combined local and global vibrations, the classification, whether local or global, is based on the higher ratio of their modal strain energy, calculated in Table 4

**Table 4** Contributions of axial and bending strain energies to the total strain energy of the first eighteen modes

| Mode | Freq. [Hz] | Axial MSE ratio $(U_a/U_t)^{1,2}$ | Bending MSE ratio $(U_b/U_t)^{1,2}$ | Vibration type | | |
|---|---|---|---|---|---|---|
| | | | | Global | Local | G & L |
| 1 | 6.61 | 0.000 | 0.995 | – | X | – |
| 2 | 6.85 | 0.000 | 0.997 | – | X | – |
| 3 | 18.02 | 0.002 | 0.995 | – | X | – |
| 4 | 18.06 | 0.000 | 0.995 | – | X | – |
| 5 | 35.32 | 0.000 | 0.995 | – | X | – |
| 6 | 35.52 | 0.000 | 0.996 | – | X | – |
| 7 | 58.02 | 0.010 | 0.986 | – | X | – |
| 8 | 58.33 | 0.000 | 0.995 | – | X | – |
| 9 | 86.99 | 0.001 | 0.992 | – | X | – |
| 10 | 87.08 | 0.002 | 0.993 | – | X | – |
| 11 | 97.54 | 0.912 | 0.062 | X | - | – |
| 12 | 121.49 | 0.000 | 0.994 | – | X | – |
| 13 | 122.28 | 0.026 | 0.969 | – | X | – |
| 14 | 127.41 | 0.928 | 0.049 | X | – | – |
| 15 | 144.50 | 0.835 | 0.150 | X | – | – |
| 16 | 161.35 | 0.006 | 0.988 | – | X | – |
| 17 | 161.85 | 0.012 | 0.981 | – | X | – |
| 18 | 191.82 | 0.472 | 0.441 | – | – | X |

[1]The summation of the strain energies ratios is not equal to one, because the contributions of shear and torsion strain energies are not included, [2]MSE is an abbreviation of modal strain energy, $U_a$ the axial modal strain energy, $U_t$ total modal strain energy, and $U_b$ is the bending modal strain energy
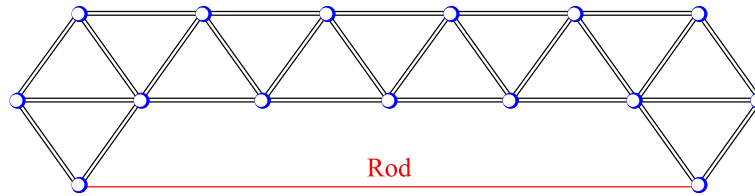


**Fig. 8** First set-up of sensors to capture global modes of the space truss structure, sensors (◯) are on the structural connection nodes

modal deformation are almost equal. Consequently, this mode is classified as a combination of global and local deformation.

Based on the numerical analysis results, it can be concluded that it should be possible to identify several modes by modal testing as global and others as local member modes. At the same time, due to relatively close natural frequencies and some mode shapes that combine local and global deformation patterns, it is a great challenge to identify some modes correctly and relate them to the numerical results.

## 5 Experimental verification

5.1 Experimental set-up

In the modal tests, 3d-accelerometers (PCB 356A16, sensitivity $\pm$ 100 mV/g) were installed in three set-ups to focus on a clear distinction between global and local vibration mechanisms. The sensors in the first set-up were positioned on the connecting structural nodes of the space truss structure to identify only global vibration modes, as shown in Fig. 8.

The second and third set-ups target the local bending vibration modes of tension and compression members, respectively, as indicated in Fig. 9. The structural response to multiple impulsive excitations, generated by means of an impulse hammer, was simultaneously recorded using the accelerometers in lateral and vertical directions. The broadband spectrum of the impulses covered a frequency range of up to approximately 220 Hz. No pre-stressing was applied to the threaded rod in any set-up configurations. For the modal identification, the SSI-cov was utilised as implemented in [16].
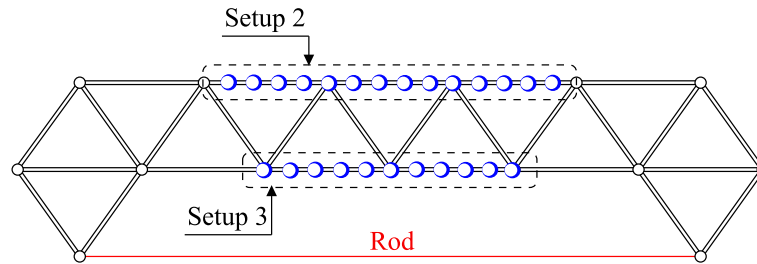
**Fig. 9** Second and third set-ups of sensors to capture local member vibration modes of the space truss structure, sensors (○) are distributed equally along the length of the members, set-up 2 is for tension top chord members, while set-up 3 is for compression bottom chord members
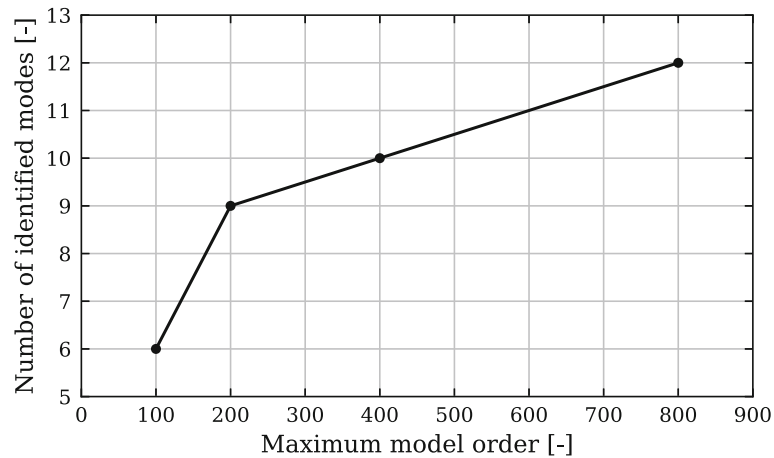


**Fig. 10** Influence of the maximal model order on the number of identified experimental modes from tests in the first set-up, number of block rows considered equals 300, (●) only these points are considered in the analysis

### 5.2 Modal identification

Prior to a modal identification, it is important to investigate the influence of the analysis parameters used within the SSI-cov, such as the number of block rows of the block-Toeplitz matrix and the maximal considered system model order, for example, as proposed in [17]. On the one hand, if the model order is underestimated, it may result in some modes being left unidentified within the considered frequency range. On the other hand, the consideration of model orders greater than the actual system model order results in spurious solutions that are not related to the physical system behaviour. Particularly in the case of space truss structures, vibration modes of non-instrumented members may contribute to the measured signals and result in identified modal solutions that are difficult to interpret.

Additional effects can occur due to interference between modes with close natural frequencies, for example, global and local modes, which is the case in this work. A stabilisation diagram is a reliable tool for selecting physical mode shapes to obtain solutions for a parametric modal identification.

Figure 10 shows the relation between the maximum model order used in the identification process and the number of obtained experimental modes. The relation between the identifiable modes and the maximum model order indicates that not only the mathematical system, to be identified in the first step of the system identification, is related to the modal model but also to a mechanical system model with a certain number of actual DOF. For example, as in this study, only a model that includes DOF between the structural connection nodes can show modes representing deformation along the truss members. Therefore, the minimum model order to identify local vibration modes is by far higher than the one required for identifying global ones, which only includes DOF at the structural connecting nodes. Nonetheless, modal contributions of the analysed measurements include the well-known effect on the minimum model order required to obtain modes that have hardly a response at the respective DOF.

The maximum model order is typically bounded by 100 or 200 for common civil engineering applications. Yet, as shown in Fig. 10, the increase in the model order leads to more identified modes. Figure 11 shows how
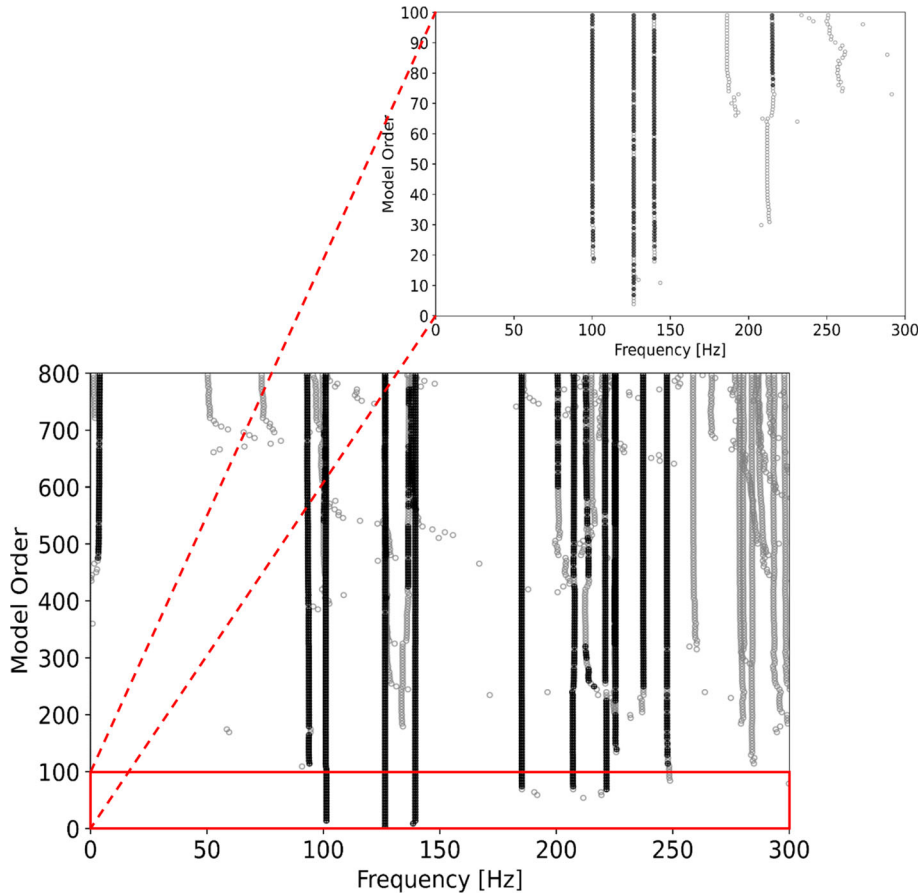
**Fig. 11** Stabilisation diagram of identified modes from tests in the first set-up; using a model order of 800 with 300 block rows and a model order of 100 with 50 block rows

insufficient the use of a model order of 100 is for identifying modal parameters of the considered space truss structure. In a range of frequencies up to 300 Hz, it is possible to extract only four or five modes. However, for the same frequency range but with a model order greater than 100, additional stable poles appear that are not only spurious solutions but are also related to the physical modes of the structure. This observation differs from the identification of continuous systems, for example, bridges, towers, and structural floors, where a smaller model order would be sufficient with the frequency range under consideration.

### 5.3 Experimental results

#### 5.3.1 Selection of physical modes from the first set-up

Figure 12 shows the stable poles, according to the stability criteria in section 2.1, for the identified modes of the space truss structure. However, not all of the stable poles are solutions related to physical modes. Thus, additional selection criteria based on the following parameters are utilised:

1. damping ratio to be positive and less than 5%,
2. mode shape complexity by modal phase collinearity (MPC) value [18] to be equal to or greater than 0.9.

Table 5 provides the selection criteria values for 15 poles, as shown in Fig. 12. Identified experimental modes 1, 2, and 3 fail to satisfy the chosen criteria to obtain physical modes. Despite this, it is worth noting that a comparison of the solutions for these modes at different model orders reveals an increase in solution accuracy with higher model orders. Thus, it may be possible to obtain solutions for these modes that meet the criteria at even a higher model order than 800. Additionally, even though these solutions are concentrated
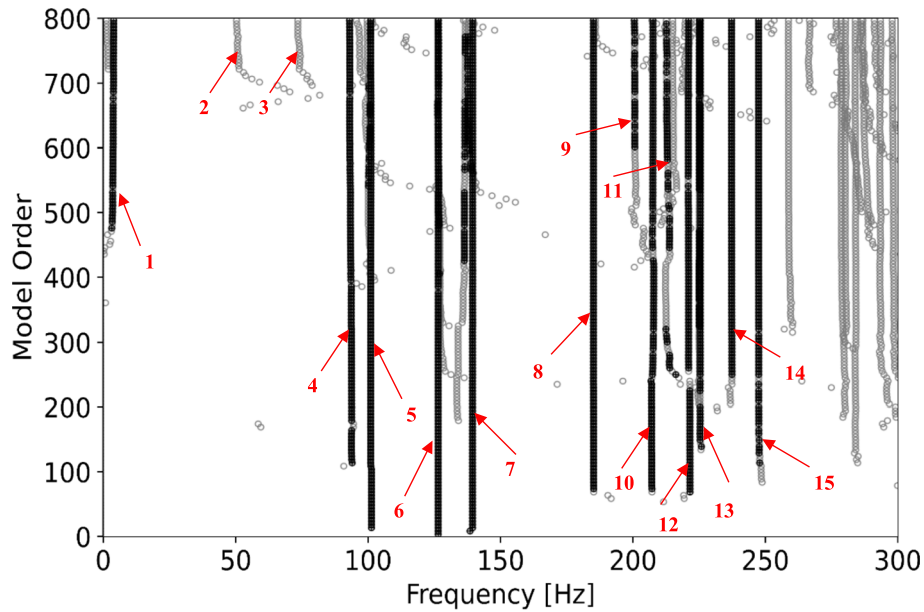
**Fig. 12** Stabilisation diagram of stable and non-stable poles for the identification of physical modes of the space truss structure from tests in the first set-up. (○) denotes poles satisfying the pre-defined stability criteria defined in Sect. 2.1, and (○) refers to poles below these criteria

**Table 5** Natural frequencies, modal damping ratios, and MPC of the poles of the identified modes from tests in the first set-up

| Mode | Exp. Freq. (Hz) | Damping ratio (%) | MPC (–) | Mode shape type |
|---|---|---|---|---|
| 1 | 3.88 | 14.34 | 0.94 | * |
| 2 | 50.21 | 4.30 | 0.84 | * |
| 3 | 73.39 | 1.26 | 0.46 | * |
| 4 | 93.30 | 0.57 | 0.99 | 1st-order torsion |
| 5 | 100.94 | 0.46 | 0.99 | 1st-order torsion |
| 6 | 126.42 | 0.06 | 0.99 | 1st-order lateral bending |
| 7 | 139.41 | 0.25 | 0.99 | 1st-order vertical bending |
| 8 | 185.04 | 0.28 | 0.99 | 2nd-order vertical bending |
| 9 | 200.65 | 0.20 | 0.92 | 2nd-order lateral bending |
| 10 | 207.49 | 0.21 | 0.99 | 2nd-order torsion |
| 11 | 212.80 | 0.35 | 0.94 | 2nd-order torsion |
| 12 | 220.85 | 0.10 | 0.99 | 2nd-order torsion |
| 13 | 225.34 | 0.07 | 0.98 | 1st-order vertical bending |
| 14 | 237.23 | 0.19 | 0.99 | 2nd-order vertical bending |
| 15 | 247.43 | 0.07 | 0.99 | 2nd-order lateral bending |

(*) The type of mode shape could not be identified because the solution's resolution was insufficient

in the region close to the local vibration of the threaded rod, according to the numerical results, a very slight global vibration of the space frame structure could be observed. For example, the 7th numerical mode may be possible to capture by the first set-up in case of considering a higher model order.

The next step was the automatic pairing of the experimental mode shapes with the numerical results, using EMAC values calculation, as explained in Sect. 2.3. For this calculation, the weighting factor Π is based on a cluster of axial DOF for each numerical mode. The EMAC values of the identified experimental modes (4th to 15th) and the numerical modes (11th to 18th) are shown in Fig. 13.

Based on the experimental results, the 4th and 5th experimental modes exhibit first-order torsion with very close natural frequencies, which strongly correlates with the 11th numerical mode. It is worth noting that the 5th experimental mode is obtained from a lower model order compared to the 4th experimental mode. This suggests that the 5th experimental mode is more likely to be a solution related to a physical mode rather than the 4th experimental mode. Therefore, the 5th experimental mode is considered to be a more reliable representation of the system's behaviour in terms of torsion.

**Fig. 13** EMAC values of identified modes, from the tests in the first set-up, and the numerical modes for an automatic pairing of the mode shapes

In a similar manner, the 8th and 14th experimental modes are second-order vertical bending, but with significantly different frequencies. These modes correlate with the 18th numerical mode, which upon closer inspection, is found to be a combination of local deformation and global vibration, refer to Fig. 7. It is important to note that the first experimental set-up only considered DOF at the structural nodes, and the weighting factor $\Pi$ was based solely on axial DOF, without considering any bending DOF. As a result, the complete shape of the 8th experimental mode may have been underestimated. Despite this limitation, based on the natural frequencies of the 8th and 14th experimental modes, the 8th experimental mode is selected to represent the second-order vertical bending behaviour of the 18th numerical mode.
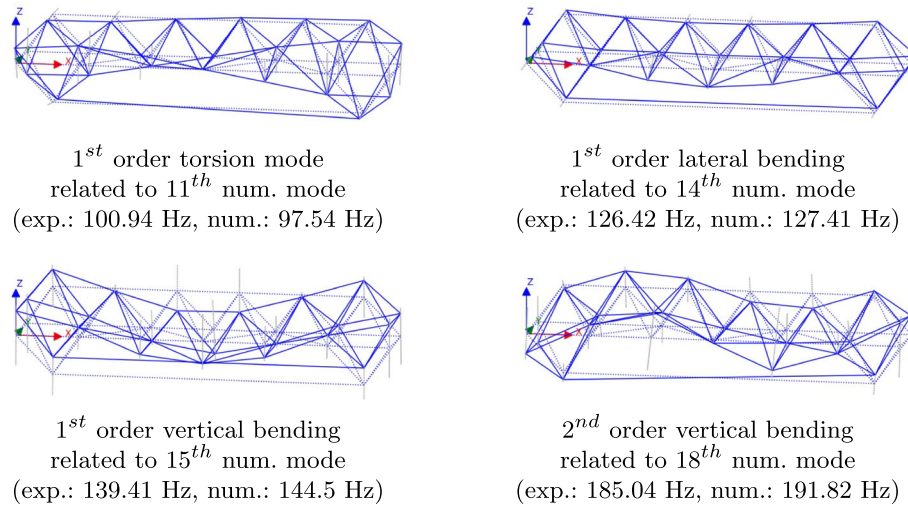
$1^{st}$ order torsion mode
related to $11^{th}$ num. mode
(exp.: 100.94 Hz, num.: 97.54 Hz)

$1^{st}$ order lateral bending
related to $14^{th}$ num. mode
(exp.: 126.42 Hz, num.: 127.41 Hz)

$1^{st}$ order vertical bending
related to $15^{th}$ num. mode
(exp.: 139.41 Hz, num.: 144.5 Hz)

$2^{nd}$ order vertical bending
related to $18^{th}$ num. mode
(exp.: 185.04 Hz, num.: 191.82 Hz)

**Fig. 14** Identified global modes of the space truss structure and their corresponding frequencies



**Fig. 15** MAC values of four global mode shapes of the space truss structure

### 5.3.2 Global modes

With accelerometers installed at the structural nodes in the first set-up, identifying global mode shapes with their frequencies was successful. Figure 14 shows four global modes within a frequency range from 90 Hz to 200 Hz. The experimental results showed a high correlation to the numerical modes, as shown in the MAC values calculated for these four modes, shown in Fig. 15.

The MAC values of the 5th, 6th, and 7th experimental modes with the 11th, 14th, and 15th numerical modes are above 90%, while for the last mode, the MAC is only 70%. As indicated in Table 4, the modal strain energy is mainly related to axial member deformations. Thus, placing the sensors at the structural nodes led to the identification of these modes with high correlation. On the contrary, in the case of the 18th numerical mode, the modal strain energy is almost equally distributed between axial and bending deformations. Consequently, an installation of sensors at both structural nodes and local members is essential to capture the full mode shape with sufficient spatial resolution. In this case, only the structural nodes were used, which explains the low MAC value of this mode.
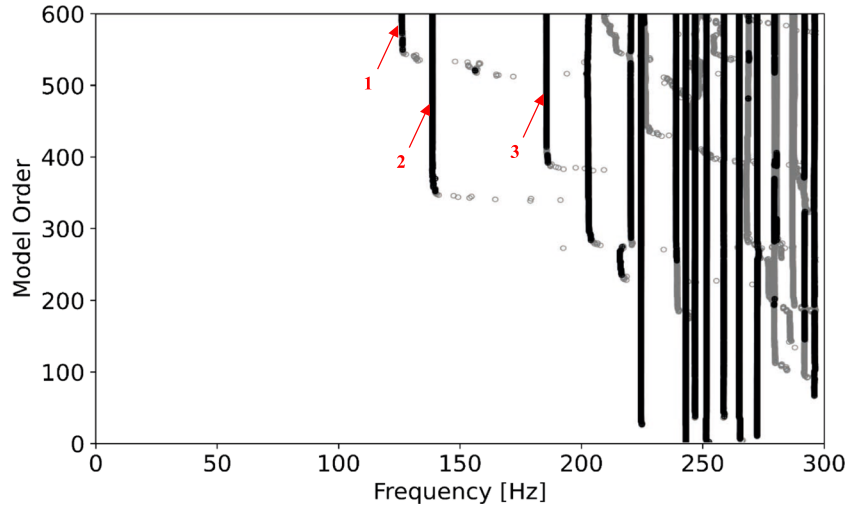
**Fig. 16** Stabilisation diagram of stable and non-stable poles for the identification of physical modes of the space truss structure from tests in the second set-up. (○) denotes poles satisfies the pre-defined stability criteria defined in Sect. 2.1, and (○) refers to poles below these criteria
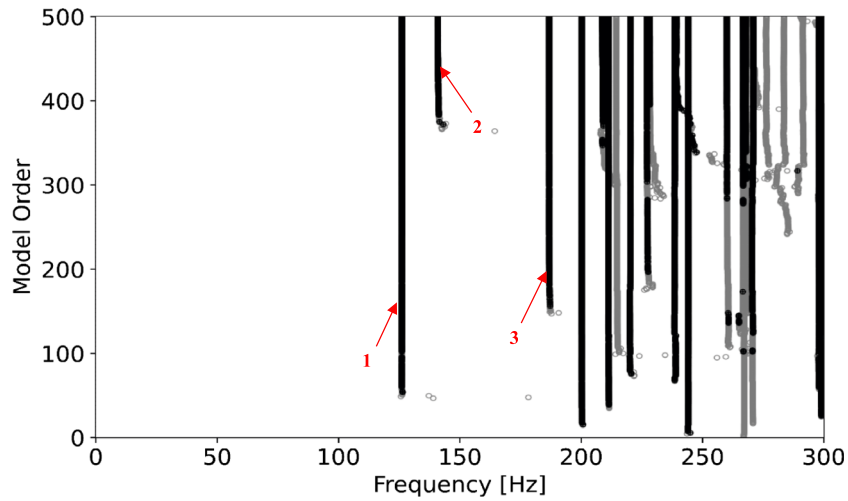


**Fig. 17** Stabilisation diagram of stable and non-stable poles for the identification of physical modes of the space truss structure from tests in the third set-up. (○) denotes poles satisfies the pre-defined stability criteria defined in Sect. 2.1, and (○) refers to poles below these criteria

**Table 6** Natural frequencies, modal damping ratios, and MPC of the poles of the identified modes from tests in the second set-up

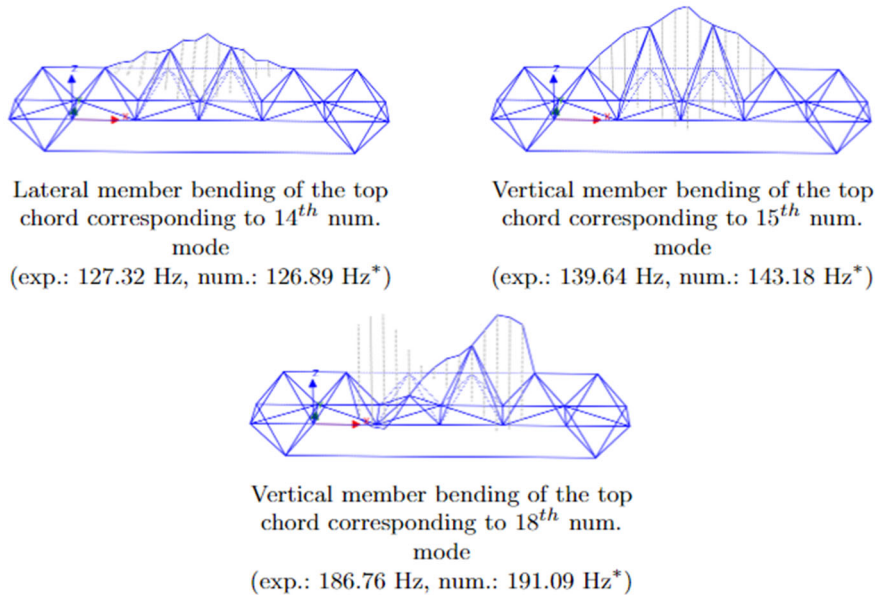| Mode | Exp. Freq. (Hz) | Damping ratio (%) | MPC (–) | Mode shape type |
|------|------|------|------|------|
| 1 | 127.32 | 0.40 | 0.99 | 1st-order lateral bending |
| 2 | 139.64 | 0.39 | 0.99 | 1st-order vertical bending |
| 3 | 186.76 | 0.11 | 0.99 | 2nd-order vertical bending |

### 5.3.3 Selection of physical modes from the two and three set-up

Figures 16 and 17 present stabilisation diagrams for the system identification of tests conducted on the second and third set-ups, respectively, to determine the local vibration modes of specific tension members in top chord and compression members in the bottom chord, as explained in Sect. 5.1.

In both cases, a high model order of 600 and 500, respectively, was required to accurately capture the local vibration modes that correspond to the global vibration behaviour of space frame structure. However, the tests,

**Table 7** Natural frequencies, modal damping ratios, and MPC of the poles of the identified modes from tests in the third set-up

| Mode | Exp. Freq. (Hz) | Damping ratio (%) | MPC (–) | Mode shape type |
|------|------|------|------|------|
| 1 | 125.92 | 0.14 | 0.99 | 1st-order lateral bending |
| 2 | 140.35 | 0.55 | 0.99 | 1st-order vertical bending |
| 3 | 186.38 | 0.09 | 0.99 | 2nd-order vertical bending |



Lateral member bending of the top chord corresponding to $14^{th}$ num. mode (exp.: 127.32 Hz, num.: 126.89 Hz$^{*}$)

Vertical member bending of the top chord corresponding to $15^{th}$ num. mode (exp.: 139.64 Hz, num.: 143.18 Hz$^{*}$)

Vertical member bending of the top chord corresponding to $18^{th}$ num. mode (exp.: 186.76 Hz, num.: 191.09 Hz$^{*}$)

**Fig. 18** Identified local member vibrations that are related to global modes of selected tension members and their frequencies. ($^{*}$) Numerical results are slightly modified to include an extra mass loading of the accelerometers and their installations, used in this set-up

in the second and the third set-ups, also showed that the local vibration mode related to the 11th numerical mode was not identified using the current model order. This finding suggests that a higher model order may be necessary to accurately capture this mode shape. Another reason is that the selected tension and compression members are in the middle of the space truss structure, while the relevant nodal DOF of the 11th numerical mode are on the four corners of the space truss, where no sensor was located in these set-ups.

Only three experimental modes for the tension and compression members' local vibrations are extracted from Figs. 16 and 17. These modes correspond to the range of the numerical results, yet more modes could be identified. The selection criteria of these modal solutions are given in Tables 5 and 6 for the local vibration modes of the tension and compression members, respectively.

### 5.3.4 Local modes

With the second and third set-ups, identifying local vibration modes that correspond to both global and local modes was possible. Figures 18 and 20 show local member vibration for tension and compression members, respectively. Experimental and numerical results of the local modes show good agreement, as given by the MAC value calculation in Figs. 19 and 21. In both cases, the identified local modes are relevant to the 14th, 15th, and 18th global numerical modes.

## 6 Conclusion

A methodology is given within this paper to identify local and global vibration modes of space frame structures. The obtained modal parameters help to determine member forces. Numerical modelling provides essential information on the expected range of frequency and the corresponding mode shapes. Estimating modal strain
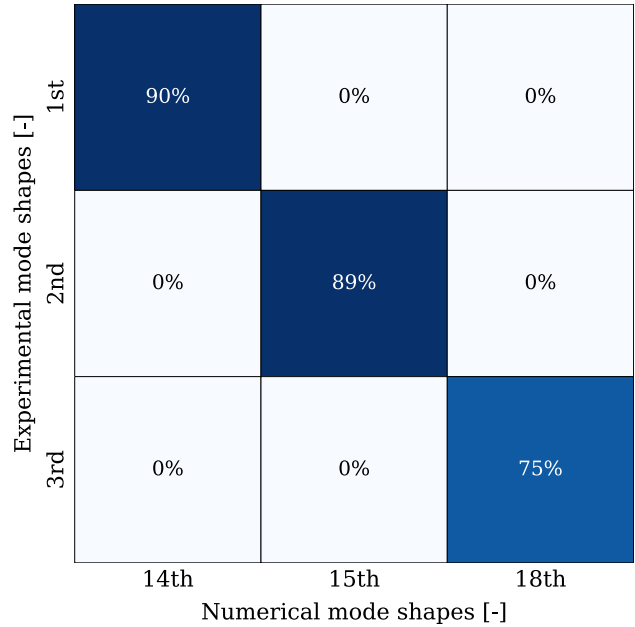
**Fig. 19** MAC values of tension members' local vibration corresponding to the three global mode shapes of the space truss structure
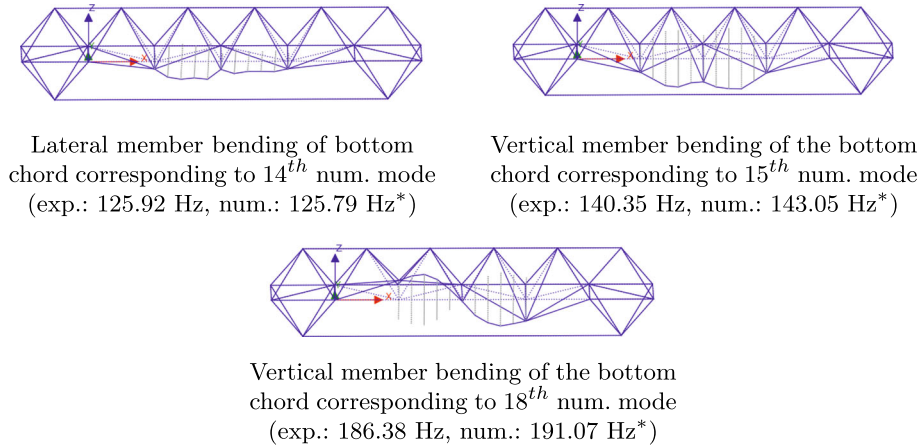


Lateral member bending of bottom chord corresponding to $14^{th}$ num. mode (exp.: 125.92 Hz, num.: 125.79 Hz$^*$)



Vertical member bending of the bottom chord corresponding to $15^{th}$ num. mode (exp.: 140.35 Hz, num.: 143.05 Hz$^*$)



Vertical member bending of the bottom chord corresponding to $18^{th}$ num. mode (exp.: 186.38 Hz, num.: 191.07 Hz$^*$)

**Fig. 20** Identified local member vibrations that are related to global modes of selected compression members and their frequencies. ($^*$) Numerical results are slightly modified to include an extra mass loading of the accelerometers and their installations, used in this set-up

energies is necessary to distinguish between local and global mechanisms of vibrations. Numerical modelling and the computation of modal strain energies facilitate the selection of DOF to be instrumented with sensors for modal testing.

Due to the high number of DOF required to describe both global and local modes of space frame structures, it is also necessary to consider comparatively high model orders in a parametric modal identification. As shown in a case study, the maximal model order to be taken into account for an identification, especially of local and combined local/global modes, can be by far higher than commonly chosen in the modal identification of typical civil structures such as bridges, towers, or floor systems.

To further improve the current understanding of the studied space truss structure, two enhancements are proposed. Firstly, it is suggested that all members of the space frame structure to be instrumented with accelerometers to fully visualise local bending deformation. Secondly, testing of a larger space frame structure is recommended to validate the applicability of current outcomes.

**Fig. 21** MAC values of compression members' local vibration corresponding to the three global mode shapes of the space truss structure

**Declarations**

**Conflict of interest** The authors declare no conflict of interest with respect to the contents of this work.

# References

1. Greening, P.D., Lieven, N.A.J.: Identification and updating of loading in frameworks using dynamic measurements. J. Sound Vib. **260**(1), 101–115 (2003). https://doi.org/10.1016/S0022-460X(02)00902-1
2. Bahra, A.S., Greening, P.D.: Identifying multiple axial load patterns using measured vibration data. J. Sound Vib. **330**(15), 3591–3605 (2011). https://doi.org/10.1016/j.jsv.2011.02.024
3. Luong, H.T.M., Zabel, V., Lorenz, W., Rohrmann, R.G.: Vibration-based model updating and identification of multiple axial forces in truss structures. Procedia Eng. **188**, 385–392 (2017). https://doi.org/10.1016/j.proeng.2017.04.499
4. Maes, K., Peeters, J., Reynders, E., Lombaert, G., Roeck, G.D.: Identification of axial forces in beam members by local vibration measurements. J. Sound Vib. **332**(21), 5417–5432 (2013). https://doi.org/10.1016/j.jsv.2013.05.017
5. Li, S., Reynders, E., Maes, K., Roeck, G.D.: Vibration-based estimation of axial force for a beam member with uncertain boundary conditions. J. Sound Vib. **332**(4), 795–806 (2013). https://doi.org/10.1016/j.jsv.2012.10.019
6. Rebecchi, G., Tullini, N., Laudiero, F.: Estimate of the axial force in slender beams with unknown boundary conditions using one flexural mode shape. J. Sound Vib. **332**(18), 4122–4135 (2013). https://doi.org/10.1016/j.jsv.2013.03.018
7. Warnaar, D.B., Mcgowan, P.E.: Effects of local vibrations on the dynamics of space truss structures. In: AIAA Dynamics Specialists Conference, pp. 868–75 (1987). https://doi.org/10.2514/6.1987-941
8. Brincker, R., Ventura, C.E.: Introduction to operational modal analysis, United Kingdom (2015)
9. Rainieri, C., Fabbrocino, G.: Operational modal analysis of civil engineering structures, New York (2014)

10. Zabel, V.: Operational modal analysis theory and aspects of application in civil engineering. Bauhaus University in Weimar, Weimar, Habilitation (2018)
11. Allemang, R.J., Brown, D.L.: A Correlation coefficient for modal vector analysis. In: Proceedings of the 1st International Modal Analysis Conference, Orlando, pp. 110–116 (1982)
12. Reynders, E., Roeck, G.D.: Reference-based combined deterministic-stochastic subspace identification for experimental and operational modal analysis. Mech. Syst. Signal Process. **22**(3), 617–637 (2008). https://doi.org/10.1016/j.ymssp.2007.09.004
13. Carrasco, C.J., Osegueda, R.A., Ferregut, C.M., Grygier, M.: Damage localization in a space truss model using modal strain energy. In: Proceedings of SPIE—The International Society for Optical Engineering, pp. 1786–1792 (1997)
14. Brehm, M., Zabel, V., Bucher, C.: An automatic mode pairing strategy using an enhanced modal assurance criterion based on modal strain energies. J. Sound Vib. **329**(25), 5375–5392 (2010). https://doi.org/10.1016/j.jsv.2010.07.006
15. SOFiSTiK AG: SOFiSTiK educational version, Germany (2018). https://www.sofistik.com
16. Marwitz, S., Zabel, V., Udrea, A.: A toolbox for operational modal analysis. The institute of structural mechanics (ISM) of the Bauhaus University in Weimar, Weimar (2007)
17. Rainieri, C., Fabbrocino, G.: Influence of model order and number of block rows on accuracy and precision of modal parameter estimates in stochastic subspace identification. Int. J. Lifecycle Perform. Eng. **1**(4), 317–334 (2014). https://doi.org/10.1504/IJLCPE.2014.064099
18. Pappa, R.S., Elliott, K.B., Schenk, A.: Consistent-mode indicator for the eigensystem realization algorithm. NASA Technical Memorandum 107607, NASA (1992). https://doi.org/10.2514/3.21092